Check for updates



# Entrainment Control Using a Newly Developed Telecentric Inline Probe

**Jonas Schulz, Kevin Schäfer, and Hans-Jörg Bart***

**DOI:** 10.1002/cite.201900112

This is an open access article under the terms of the Creative Commons Attribution License, which permits use, distribution and reproduction in any medium, provided the original work is properly cited.

This contribution presents a novel approach to investigate entrainment in distillation and absorption columns. An image-based probe allows precise droplet detection at various radial and axial positions above trays. Validations achieve an average error of 6.4 % (monospheres 9.2–114.4 µm) and 3 % (monodisperse droplet stream up to 19 m s$^{-1}$ and 74.5 µm). Experiments in a DN 450 cold flow test rig show an increasing (decreasing) share of larger droplets with higher gas (liquid) loads. Locally measured droplet sizes depend on probe position as well as tray design and enable an extrapolation to integral entrainment rates.

**Keywords:** Absorption, Distillation, Entrainment, Optical droplet measurement

*Received:* August 01, 2019; *revised:* October 25, 2019; *accepted:* November 20, 2019

## 1 Introduction

In chemical engineering distillation and absorption are the working horses in industrial separation processes [1]. Liquid entrainment reduces the separation efficiency of these processes [2] and constitutes a serious threat to connected downstream equipment [3, 4]. Entrainment represents a phase slip in countercurrent columns [5]. In this case, the gas flow entrains liquid droplets from lower to upper separation stages resulting in a recycling of liquid and a rescission of the previously achieved separation effect [6]. Today, plant designers use heuristic methods to estimate the amount of entrained liquid between stages. Nevertheless, these methods suffer from a limited range of validity concerning column dimensions, flow rates and chemical systems [7]. Therefore, the capability to precisely assess and control liquid entrainment holds a great potential to lower energy and construction costs of distillation and absorption columns [8, 9].

Conservative methods of entrainment investigation such as applying a capture tray at the column top [10] or mixing a non-volatile tracer into the liquid flow [11] lack in either accuracy or practicability. Detection and analysis of entrained liquid by optical measurement technology represents a less invasive and more cost-efficient alternative. In this contribution, the recently presented modified optical multimode online probe (OMOP) [12–14] demonstrates the capability to identify the dependency of the droplet regime on operation parameters and tray design of the column. Telecentric illumination and lenses allow precise measurements in short time using a probe with small diameter. Measurements performed according to the shadowgraphic principle by application of a transmitted light configuration generate images with high contrast, which are very suitable for further image processing [12]. In scope of this contribution, validation measurements are performed to prove the accuracy of the modified OMOP in detecting motionless but also highly dynamic particle systems. Monodisperse particle systems serve as a validation standard for detection of static and small objects. Droplets ejected from a high precision droplet generator serve as a validation standard for small and at the same time very dynamic systems. A DN 450 cold flow test rig enables the investigation of entrained liquid above different internals (sieve and fixed valve tray, RMPS 250 packing, 50 mm Pall rings). A measurement section with four positions at different heights allows axial and radial positioning of the modified OMOP above the tray. A capture tray locks up the column top. A comparison between this conservative method and the modified OMOP constitutes a central part of this contribution and proves the capability to estimate the amount of entrained liquid with experiments referring to single locations within the column.

## 2 Theoretical Background

On microscale, entrainment between stages equals the behavior of single droplets surrounded by air. Based on this idea, Souders and Brown [15] develop a force equilibrium between drag and buoyancy force acting on a single droplet.

Jonas Schulz, Kevin Schäfer, Prof. Dipl.-Ing. Dr. techn. Hans-Jörg Bart
bart@mv.uni-kl.de
Technische Universität Kaiserslautern, Chair of Separation Science and Technology, Gottlieb-Daimler-Straße 44, 67663 Kaiserslautern, Germany.

 © 2019 The Authors. Published by WILEY-VCH Verlag GmbH & Co. KGaA, Weinheim 

Foundations of this equilibrium are located in the work of de Villamil [16], who performed first experiments with solid particles floating in a stream of air.

$$\frac{\pi g d^3}{6}\left(\rho_l - \rho_g\right) = \frac{k\rho_l \pi d^2}{4} v^2 \tag{1}$$

The variable $d$ represents the diameter of the droplet, while $\rho_l$ and $\rho_g$ sum up for the densities of the liquid and gaseous phase, respectively. The resistance coefficient $k$ considers the droplet shape and by that the available windage for the buoyancy force. The velocity $v$ of the surrounding medium, where a droplet of a specific size is floating, can be defined as.

$$v = \sqrt{\frac{2gd}{3k}}\left(\frac{\rho_l - \rho_g}{\rho_g}\right)^{0.5} \tag{2}$$

If $v$ declines, the droplet falls, while an increase of $v$ results in a droplet lift. Proceeding from this relation, a critical flow factor $F_{crit} = v\rho_l^{0.5}$ predicts where a droplet is just floating before being entrained.

The excess of entrainment is clearly determined by the flow regime on a tray [11]. The most relevant flow regimes for industrial separations are froth and spray [17]. The froth regime consists of a dispersed gas phase and a continuous liquid phase, while dispersed liquid in a continuous gas phase represents the spray regime. Both regimes are marked off by a transition zone showing characteristics of both regimes [9]. In general, an increased gas load changes the regime from froth to spray [10] resulting in higher rates of entrainment [11]. By now, many authors have identified factors influencing entrainment rates with aid of a capture tray. An increase of entrainment by an increased gas load is clearly identified [1, 15, 18, 19]. The influence of the liquid load is more complex, but it is expected that low (high) liquid loads cause higher (lower) entrainment rates [9, 11]. Concerning column design, reduced tray spacing $H$ [9, 20] and fractional hole area $A_f$ [10, 21] generate higher entrainment rates. The influence of substance properties like surface tension and viscosity is by now not completely resolved [1, 18, 20, 22, 23]. Quantification of entrained liquid at the column top usually refers to either gas flow or liquid flow rates above the tray [15]. Applied for tray capacity estimation, $E_{cap}$ defines the ratio of entrained liquid $\dot{L}'$ from the respective tray to the vapor flow $\dot{V}$ passing through the tray. For the assessment of tray efficiency, $E_{eff}$ defines the ratio of entrained liquid $\dot{L}'$ from the tray to the liquid flow across the tray $\dot{L}$ [1].

$$E_{cap} = 100\frac{\dot{L}'}{\dot{V}} \tag{3}$$

$$E_{eff} = 100\frac{\dot{L}'}{\dot{L}} \tag{4}$$

Entrainment rates $E_{eff}$ up to 5 % are often tolerated [9] but can significantly diminish the separation efficiency of mixtures with high volatility, where the concentration profiles between each stage vary significantly from each other. Capture trays represent the most prevalent measurement method to investigate the influence of operation parameters on entrainment rates [2, 24]. Advantages of this method are the generation of reproducible rates and an acceptable installation effort. Droplets hitting the tray bottom and falling back down constitute a systematic measuring error of this method [11]. In addition, experiments with a capture do not refer to the standard operation procedure of the column, as used capture trays have to be dismounted and replaced by regular trays for high heat and mass transfer. Therefore, correlations originating from capture tray experiments are not fully applicable to industrial scale columns [6].

Using a non-volatile tracer mixed in the liquid flow entering the second last tray represents an alternative approach to estimate entrainment [25]. By introducing a mass balance around the last tray including the concentration differences of the tracer Lockett et al. [11] precisely assess entrainment rates under process conditions. A disadvantage of this method is the extra effort and expense with respect to the test rig and the limited practicability with respect to industrial systems. Both methods pursue an integral approach, while optical and impingement measurement techniques represent local measurement methods within the column.

Impingement methods use a plate covered with a thin film (e.g., magnesium oxide), which enables droplet detection by measurement of spots or craters in the film after removal of the plate from the column [7, 21, 26]. These methods require a small amount of effort for execution but more for later analysis, especially with respect to a large number of experiments. Optical measurement techniques are able to reduce this amount of effort due to computer-assisted data handling and analysis. For example, phase Doppler anemometry (PDA) is capable of detecting and analyzing droplets precisely in terms of size and velocity. Limited industrial applicability due to high calibration and measurement efforts, spatial and local requirements of the measurement access and specific instruction in respect of safety and explosion protection represent the many downsides [27, 28].

A successful detection and analysis of entrained droplets above sieve trays [14] demonstrates the applicability of imaging methods for investigation of dispersed fluid flows. First deployment of an imaging method to investigate entrained liquid goes back to Pinczewski and Fell [29], who combined a camera probe inside a rectangular column with an electronic flash outside the column wall. In general, imaging methods are flexible in respect of application and measurement access. Measurements can take place directly inside the column with tolerable extent of invasivity, which declines with smaller outer dimensions of the imaging device. Measurement systems based on transmitted light

 © 2019 The Authors. Published by WILEY-VCH Verlag GmbH & Co. KGaA, Weinheim 

15222640, 2020, 3, Downloaded from https://onlinelibrary.wiley.com/doi/10.1002/cite.201900112 by Rheinland-Pfälzische Technische Universität Kaiserslautern-Landau, Wiley Online Library on [05/04/2024]. See the Terms and Conditions (https://onlinelibrary.wiley.com/terms-and-conditions) on Wiley Online Library for rules of use; OA articles are governed by the applicable Creative Commons License

and telecentric optics require a slightly higher installation effort in terms of two measurement access points placed diametrically to each other. The positioning of camera unit and light source generates shadowgraphic images with highest contrast, facilitating the subsequent image evaluation including low calibration and measurement efforts [30, 31]. For large diameter columns and even lower installation effort an endoscopic version of a shadowgraphic probe was developed, which can be operated using just one existing nozzle at the column shell [32].

## 3 Measurement Methods and Validation Standards

The modified OMOP consists of a camera and illumination unit. A dimmable LED provides a light flux between 700 and 1400 lm for a free adjustment of image illumination. The camera unit is equipped with a matrix camera (Basler ace series) and a telecentric lense (Edmund Optics CompactTL™ Series), which is suitable for distance-independent imaging of droplets within the measurement volume. Positioning and setup of the illumination unit guarantee a telecentric illumination generating equally illuminated and high-contrast images of entrained droplets based on the fundamental principle of Köhler [33]. The substantial difference to the initially introduced instrument [34] is a shielding tube resulting in a set back of the hydrophobically coated inspection windows, which prevent droplets from coalescing at the window. Furthermore, a pneumatic purging system enables the removal of coalesced droplets from the inspection windows under harsh process conditions. A detailed outline of the modified OMOP is depicted in [12]. Monodisperse glass particles in scale from 9.2 µm to 114.4 µm (Whitehouse Scientific Ltd) serve as a validation standard for small and unmoved objects. A high precision droplet generator (FMP Technology GmbH) ejects monodisperse droplets with high velocities (10.9–19 m s$^{-1}$) in scale from 74.5 µm to 200.8 µm serving as a validation standard for small but also fast moving objects. A variation of the camera exposure time (1–7 µs) demonstrates the minimum required exposure time to image small and fast moving objects. Fig. 1 illustrates the image acquisition of the immobile particle systems (Fig. 1a) and the acquisition of highly dynamic droplet streams at different exposure times (Fig. 1b).

Schulz and Bart [14] already cover a successful comparison between modified OMOP and PDA in a DN 200 spray column. In order to achieve a comparison between capture tray and modified OMOP, the locally detected droplet volume is extrapolated to an integral amount of entrained liquid. This extrapolation considers the detected droplet volume $V_d$ in dependence on measurement volume $V_{meas}$, distance between probe and capture tray $H_{cap}$, tray bubbling area $A_b$, covered area by modified OMOP $A_{OMOP}$, and acquisition rate $f_{cam}$. The following relation describes the extrapolation in brief.

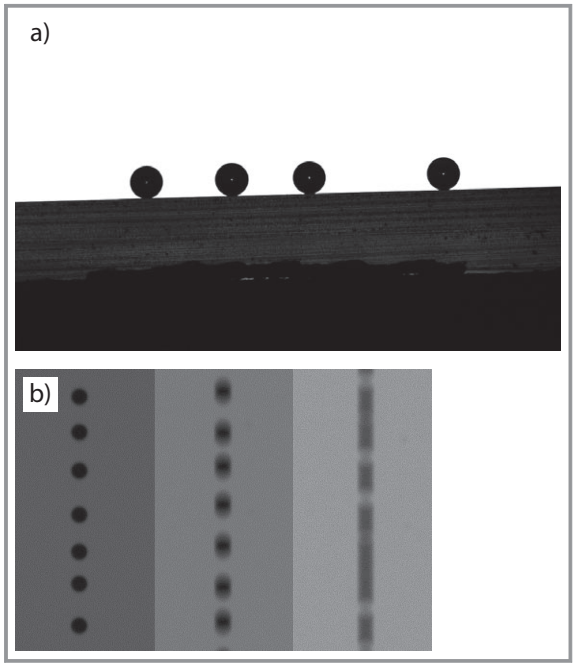


**Figure 1.** a) Front view on monospheres, b) effect of exposure time on focus.

$$\dot{E}' = V_d f\left(V_{meas}, H_{cap}, A_b, A_{OMOP}, f_{cam}\right) \tag{5}$$

Eq. (6) is calculated with the extrapolated entrainment rate $\dot{E}'$ instead of the quantified $\dot{L}'$ from Eq. (4) to acquire a comparison between extrapolated entrainment rates from the modified OMOP and experimentally quantified entrainment rates from the capture tray.

$$E_{eff} = 100\frac{\dot{E}'}{\dot{L}} \tag{6}$$

The definition of $E_{cap}$ is acquired in the same way.

## 4 Experimental Test Rig

A DN 450 ($A_c$ = 0.164 m$^2$) glass column (DE Dietrich Process Systems GmbH) in combination with the aforementioned measurement section (RVT PE GmbH) and capture tray (Raschig GmbH) represents the test rig relevant for this contribution. The column holds a number of maximum three trays (sieve and fixed valve; RVT PE GmbH) with a constant spacing of 500 mm. An operation with 1.5 m of structured (RMP S250; RVT PE GmbH) or random packings (Pall rings, 50 mm; Envimac Engineering GmbH) is also possible and planned for later contributions. Investigations on sieve ($d_h$ = 11 mm; $A_b$ = 0.139 m$^2$; $A_f$ = 5.7 %) and fixed valve ($h_{valve}$ = 10 mm; $A_b$ = 0.139 m$^2$; $A_f$ = 6.7 %) trays run at 293.15 K room temperature and constant outlet weir settings of 0.05 m height $h_w$ and 0.24 m length $l_w$. A gas flow inlet positioned vertical to the column bottom achieves an

 © 2019 The Authors. Published by WILEY-VCH Verlag GmbH & Co. KGaA, Weinheim 

15222640, 2020, 3, Downloaded from https://onlinelibrary.wiley.com/doi/10.1002/cite.201900112 by Rheinland-Pfälzische Technische Universität Kaiserslautern-Landau, Wiley Online Library on [05/04/2024]. See the Terms and Conditions (https://onlinelibrary.wiley.com/terms-and-conditions) on Wiley Online Library for rules of use; OA articles are governed by the applicable Creative Commons License

almost homogenous distribution starting from the first tray. A high-pressure radial blower (Elektror Airsystems GmbH; HRD 60 FUK) provides the gas flow inlet with unsaturated air. The gas flow is saturated by the liquid phase on the tray. Already low gas flows of 1.0 $Pa^{0.5}$ and low liquid flows across the last tray of 6.3 $m^3m^{-1}h^{-1}$ increase the humidity of the gas phase up to 99 % approx. 25 min after test rig start. A centrifugal pump (KSB AG; Movitec V2-5) delivers the liquid flow from the column sump to the top, where it enters the inlet area (inlet weir height 0.5 m). Liquid loads up to 25 $m^3m^{-1}h^{-1}$ and gas factors up to 3.0 $Pa^{0.5}$ allow operation over the complete design range of both trays. For this article, liquid load refers to the liquid flow rate per meter of outlet weir length $l_w$. Tab. 1 summarizes the liquid flow rates relevant for this contribution in $m^3m^{-1}h^{-1}$ and in $m^3m^{-2}h^{-1}$ for comparability with experiments in packed columns, where liquid flows refer to column cross-sectional area $A_c$.

**Table 1.** Liquid loads related to outlet weir length in $m^3m^{-1}h^{-1}$ ($l_w$ = 0.24 m) and column cross sectional area in $m^3m^{-2}h^{-1}$ ($A_c$ = 0.164 m).

| Liquid flow per meter weir length [$m^3m^{-1}h^{-1}$] | Liquid flow per column cross-sectional area [$m^3m^{-2}h^{-1}$] |
|---|---|
| 4.2 | 6.1 |
| 6.3 | 9.1 |
| 8.3 | 12.2 |
| 10 | 14.6 |
| 15 | 21.9 |
| 20 | 29.3 |
| 25 | 36.6 |

The measurement section (1.4307) contains four inlets, each on an individual height (57.5 mm, 152.5 mm, 247.5 mm and 342.5 mm) to capture droplet size distributions (DSD) with the modified OMOP at varying axial and radial positions above the last tray. The capture tray is positioned 0.5 m above the last tray and locks up the column top. A demister mesh pad positioned 0.25 m above the capture tray prevents entrainment of very small and fast droplets. A detailed outline of the test rig is depicted in [12, 14].

## 5 Results and Discussion

### 5.1 Validation Results

The validation measurements of the modified OMOP with the aforementioned monodisperse glass particles are depicted in Fig. 2 including the monosphere diameters provided by the manufacturer as a 45° line through the origin of the coordinate system. Measurements with the modified OMOP show only minor deviations from the manufacturer

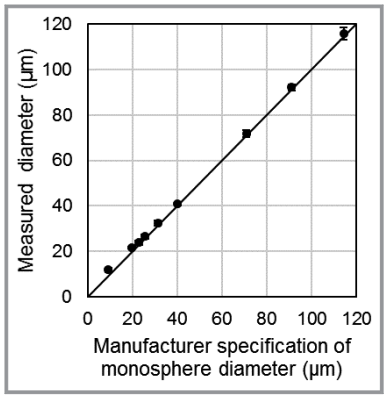


**Figure 2.** Validation of modified OMOP with immobile monodisperse glass particles.

specifications. As expected, these deviations increase with a decrease in particle size. Tab. 2 summarizes the measurement results including standard deviation $s$ and a relative measurement deviation $f_x$ from the manufacturer specifications.

**Table 2.** Detailed measurement results of OMOP validation with monodisperse glass particles.

| Manufacturer specification | | Experimental results | | |
|---|---|---|---|---|
| $d$ [µm] | $s$ [µm] | $d_{exp}$ [µm] | $s_{exp}$ [µm] | $f_x$ [%] |
| 114.4 | 2.6 | 115.9 | 2.7 | 1.3 |
| 91.2 | 0.9 | 92.1 | 1.3 | 1 |
| 70.9 | 0.8 | 72 | 1.6 | 1.5 |
| 40.2 | 0.5 | 41.0 | 0.9 | 2.1 |
| 31.3 | 0.8 | 32.4 | 1.2 | 3.3 |
| 25.6 | 0.7 | 26.5 | 1.0 | 3.7 |
| 22.8 | 0.8 | 23.8 | 1.0 | 4.5 |
| 19.7 | 0.2 | 21.6 | 0.4 | 9.9 |
| 9.2 | 0.2 | 12.0 | 1 | 30.2 |

The results show a precise detection of the monodisperse particles with the modified OMOP. Solely particles smaller than 10 µm are difficult to detect and thus result in stronger average deviations from the manufacturer specifications. Nevertheless, relative measurement deviation across all samples amounts to merely 6.4 %. It must be mentioned, that the capability to detect even smaller particles with higher accuracies will be most likely possible in the future with even more efficient camera models, due to the rapidly growing demand for industrial image processing. Validation measurements with the droplet generator are successfully performed for monodisperse droplet streams of 200.8 µm ($f_x$ = 4.9 %), 138.5 µm ($f_x$ = 2.3 %) and 74.5 µm ($f_x$ = 1.8 %) in diameter. Ejection velocities sum up to 10.9 m $s^{-1}$

 © 2019 The Authors. Published by WILEY-VCH Verlag GmbH & Co. KGaA, Weinheim 

15222640, 2020, 3, Downloaded from https://onlinelibrary.wiley.com/doi/10.1002/cite.201900112 by Rheinland-Pfälzische Technische Universität Kaiserslautern-Landau, Wiley Online Library on [05/04/2024]. See the Terms and Conditions (https://onlinelibrary.wiley.com/terms-and-conditions) on Wiley Online Library for rules of use; OA articles are governed by the applicable Creative Commons License

(200.8 µm), 14.1 m s$^{-1}$ (138.5 µm) and 19 m s$^{-1}$ for the smallest droplet of 74.5 µm in diameter. Furthermore, an investigation on the droplet detection accuracy in dependence on the exposure time was carried out for the droplet diameter of 74.5 µm at a velocity of 18.9 ms$^{-1}$ to guarantee a reliable image analysis under experimental conditions. Results show that a low exposure time is required for precise detection of fast moving liquid droplets. In this case, the relative measurement deviation $f_x$ for exposure times of 1–4 µs remains below 9^%, while for example the highest exposure time of 7^µs results in larger deviations ($f_x$ = 27.1 %). It must be mentioned, that this validation test pushes the modified OMOP towards its limits. The DN 450 test rig, relevant for this contribution runs at gas factors up to a maximum of 3 Pa$^{0.5}$. In conclusion, droplets erupting out of the liquid phase are most likely slower than the here demonstrated 18.9 ms$^{-1}$. Nevertheless, the following measurements are performed at an exposure time of 4 µs to guarantee a precise imaging of the entrained droplets.

## 5.2 Experimental Results from DN 450 Test Rig

Entrainment quantifications with capture tray are depicted in Fig. 3 for the sieve and fixed valve tray, respectively. For practicability reasons, entrainment rates over 10 % are not included in these charts, as the progressions of the graphs give a well estimation of the expected increase of entrainment rates by an increase of the respective gas or liquid load.

The results reveal two effects. At first, entrainment rates increase with increasing gas loads, which is in line with the findings of many authors [1, 15, 18, 19]. Considering Eq. (1) and (2), this behavior appears reasonable as higher gas loads increase the buoyancy force acting on each liquid droplet. This leads to an uplift of larger droplets to higher levels above the tray and by that an increase of entrainment rates. Secondly, higher liquid loads consistently decrease the amount of entrained liquid. According to Staak [4] this behavior is expected, as a higher amount of liquid on the tray results in a broader energy dissipation of the gas flow. Consequently, droplets erupting out of the liquid phase hold less kinetic energy and will less often reach the next tray. Examination of the pressure drop across the trays supports this expectation. For example, dry sieve tray pressure drop amounts to 1.3 mbar at 1 Pa$^{0.5}$ and goes up to 2.8 mbar at 1.5 Pa$^{0.5}$. Liquid loads of 10 m$^3$m$^{-1}$h$^{-1}$ further increase the pressure drop to 5.8 mbar at 1.0 Pa$^{0.5}$ and 9.2 mbar at 1.5 Pa$^{0.5}$. The reduction of kinetic energy can also be indirectly observed by the modified OMOP. For example, the detected quantity of droplets above the sieve tray is reduced by 53 % if liquid loads rise from 10 m$^3$m$^{-1}$h$^{-1}$ to 25 m$^3$m$^{-1}$h$^{-1}$ at a constant gas load of 1.5 Pa$^{0.5}$. Nevertheless, a third effect becomes apparent on both trays at high liquid loads of 15 m$^3$m$^{-1}$h$^{-1}$. Entrainment rates still decrease but change faster to high shares of more than 10 %. The rapid change of entrainment rates is based on the limited downcomer capacity and becomes apparent by a downcomer flooding, which increases at operation areas of high liquid loads of 20 and 25 m$^3$m$^{-1}$h$^{-1}$. Authors who performed experiments over the whole tray design area with respect to gas and liquid load capacities observed this effect as well [6, 11]. A comparison between Fig. 3a and 3b shows lower entrainment rates across all gas and liquid loads with respect to the fixed valve tray. This behavior appears reasonable, as the hole area of the sieve tray points directly vertical towards the bottom of the capture tray. Gas flowing through the holes is not deflected in contrast to the fixed valve tray, where the opening of the valve points directly vertical towards the column wall. Due to deflection and the smaller dimension of the sieve hole ($A_{h,sieve\ hole}$ = $9.5 \cdot 10^{-5}$ m$^2$) compared to fixed valve construction ($A_{h,valve}$ = $6.4 \cdot 10^{-4}$ m$^2$) the gas flow is able to penetrate the froth phase with a higher velocity with respect to the sieve tray. Subsequently, droplet emergence intensifies resulting in higher rates of entrainment.

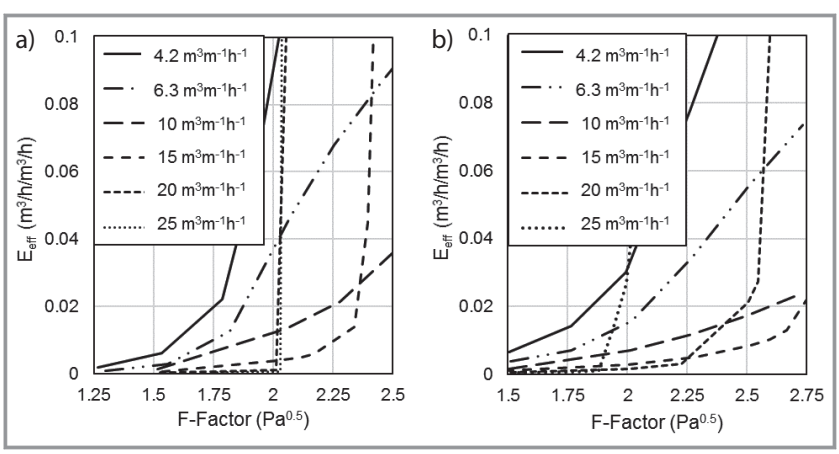


**Figure 3.** a) $E_{eff}$ sieve tray to 25 m$^3$m$^{-1}$h$^{-1}$ and 2.5 Pa$^{0.5}$, b) $E_{eff}$ fixed valve tray to 25 m$^3$m$^{-1}$h$^{-1}$ and 2.75 Pa$^{0.5}$.

The modified OMOP measurements depicted in Fig. 4a show the effect of an increased gas load on DSD 342.5 mm above the sieve tray at a liquid load of 10 m$^3$m$^{-1}$h$^{-1}$. Results show larger droplet sizes for higher gas loads. For example, at 1.5 Pa$^{0.5}$ the share of droplets below 1000 µm accounts for 82 % of the total droplet volume, while at 2.0 Pa$^{0.5}$ the same range of droplet sizes comes to a share of only 62 %. Based on theoretical considerations of Souders and Brown [15] and the capture tray measurements (Fig. 3), an increase of the droplet size is expected as a higher gas load is able to lift larger droplets on higher positions above the tray. Calculation of the critical flow factor $F_{crit}$ based on Eq. (2) gives

 © 2019 The Authors. Published by WILEY-VCH Verlag GmbH & Co. KGaA, Weinheim 

15222640, 2020, 3, Downloaded from https://onlinelibrary.wiley.com/doi/10.1002/cite.201900112 by Rheinland-Pfälzische Technische Universität Kaiserslautern-Landau, Wiley Online Library on [05/04/2024]. See the Terms and Conditions (https://onlinelibrary.wiley.com/terms-and-conditions) on Wiley Online Library for rules of use; OA articles are governed by the applicable Creative Commons License

$F_{crit,1}$ = 2.17 $Pa^{0.5}$ for a median droplet diameter of $x_{50}$ = 560 µm for the experiment at 1.5 $Pa^{0.5}$. Consequently, a gas factor higher than 2.17 $Pa^{0.5}$ will most likely entrain droplets larger than 560 µm. The critical flow factor for 2.0 $Pa^{0.5}$ is $F_{crit,2}$ = 2.61 $Pa^{0.5}$ for $x_{50}$ = 810 µm. Increased gas loads will entrain more droplets larger than 810 µm, which is clearly recognizable by comparing both curves. In conclusion, the share of larger droplets detected by the modified OMOP rises with increasing gas loads. Schulz and Bart [14] show the same effect for gas factors of 1.54 $Pa^{0.5}$ and 1.94 $Pa^{0.5}$ above a sieve tray at a low liquid load of 1.06 $m^3m^{-1}h^{-1}$. In order to prove that this behavior is consistent across the whole tray design area, measurements at higher liquid loads are depicted in Fig. 4b (20 $m^3m^{-1}h^{-1}$) for the sieve tray and in Fig. 5a (20 $m^3m^{-1}h^{-1}$) and 5b (25 $m^3m^{-1}h^{-1}$) for the fixed valve tray. Again, the measurement height was set to 342.5 mm between tray bottom and modified OMOP in order to guarantee comparability.

The behavior of the DSD in response to an increased gas load remains consistent across all liquid loads and both trays types. Even experiments at 25 $m^3m^{-1}h^{-1}$ close to downcomer flooding (see Fig. 5b) generate larger droplets at higher gas loads. For example, in Fig. 5a, half of the entrained liquid volume are droplets ≤ 1010 µm for a gas factor of 2.0 $Pa^{0.5}$. At 1.5 $Pa^{0.5}$ the same share consists of droplets ≤ 500 µm or droplets ≤ 315 µm in case of the low gas factor of 1.0 $Pa^{0.5}$. These results combined with the findings of Schulz and Bart [14] underline the consistency of the gas load effect, which becomes apparent by the increase of the large droplet share above a tray with increasing gas loads both in low and high areas of liquid loads. As mentioned before, the effect of liquid load on entrainment is not completely clarified [2, 6, 11]. Therefore, DSD above both trays at different liquid loads serve as an alternative explanation attempt.

Fig. 6 depicts DSD up to 25 $m^3m^{-1}h^{-1}$ at 1.5 $Pa^{0.5}$ with respect to a measurement height of 342.5 mm above the sieve tray. The results show a decrease of the droplet size with an increasing liquid load. Graphs at 6.3 and 8.3 $m^3m^{-1}h^{-1}$ show an almost equal progression, which indicates that only wide changes of the liquid load lead to relevant differences in the respective DSD. For better recognition, the graph for a liquid load of 6.3 $m^3m^{-1}h^{-1}$ is depicted with a smaller line width. Furthermore, the graph for 25 $m^3m^{-1}h^{-1}$ shows a marginal share of larger droplets compared to measurements at 20 $m^3m^{-1}h^{-1}$. Referring to Kister and Haas [6] as well as Lockett et al. [11] this effect appears reasonable, as entrainment rates first decrease with rising liquid loads and then start to increase again at high liquid loads. An analysis of the arithmetic mean diameter confirms this assumption. Average droplet diameters amount to $\bar{x}$ = 147 (146) µm at 6.3 (8.3) $m^3m^{-1}h^{-1}$ and decrease to $\bar{x}$ = 63 µm at 20 $m^3m^{-1}h^{-1}$. Measurements at 25 $m^3m^{-1}h^{-1}$ show again a slight increase of the arithmetic mean to 77 µm. For reasons of clarity and comprehensibility, Fig. 7 summarizes the large amount of DSD for the fixed valve tray into a single detected droplet size for each DSD based on the arithmetic mean.

The fixed valve tray also shows a decline of the droplet size with increasing liquid loads followed by an increase of the average droplet size at 2.0 $Pa^{0.5}$. As can be seen in Fig. 3b an increase of entrainment at 2.0 $Pa^{0.5}$ is reasonable, as the capture tray measurements above the fixed valve tray show an increased amount of entrainment at 2.0 $Pa^{0.5}$ and 25 $m^3m^{-1}h^{-1}$. Measurements at 1.0 and 1.5 $Pa^{0.5}$ and 20–25 $m^3m^{-1}h^{-1}$ show a decrease as entrainment in Fig. 3b is also decreasing and not yet increasing as the gas factor is still too low to entrain a relevant amount of liquid. In conclusion, measurements above both trays show a decrease of the average droplet diameter with increasing liquid loads independent of the investigated gas load. Increasing liquid load near to the design area of downcomer flooding can again increase the average droplet size and, thus,

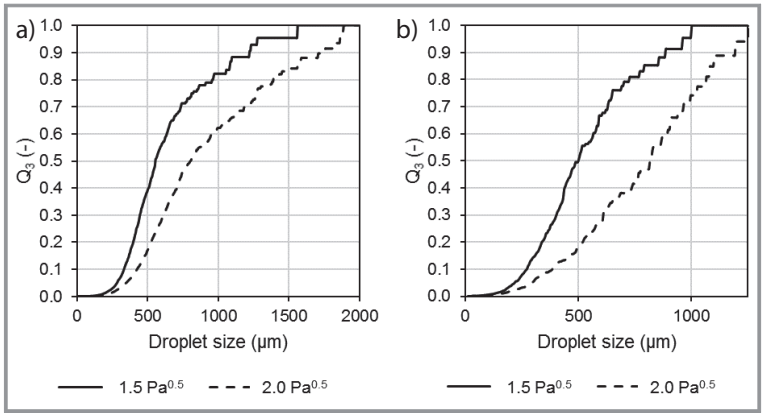


**Figure 4.** Gas load effect on DSD above sieve tray at a) 10 $m^3m^{-1}h^{-1}$ and b) 20 $m^3m^{-1}h^{-1}$.

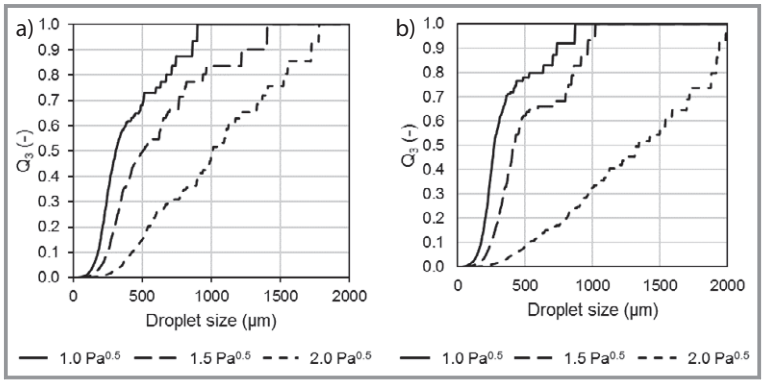


**Figure 5.** Gas load effect on DSD above fixed valve tray at a) 20 $m^3m^{-1}h^{-1}$ and b) 25 $m^3m^{-1}h^{-1}$.

 © 2019 The Authors. Published by WILEY-VCH Verlag GmbH & Co. KGaA, Weinheim 

15222640, 2020, 3, Downloaded from https://onlinelibrary.wiley.com/doi/10.1002/cite.201900112 by Rheinland-Pfälzische Technische Universität Kaiserslautern-Landau, Wiley Online Library on [05/04/2024]. See the Terms and Conditions (https://onlinelibrary.wiley.com/terms-and-conditions) on Wiley Online Library for rules of use; OA articles are governed by the applicable Creative Commons License

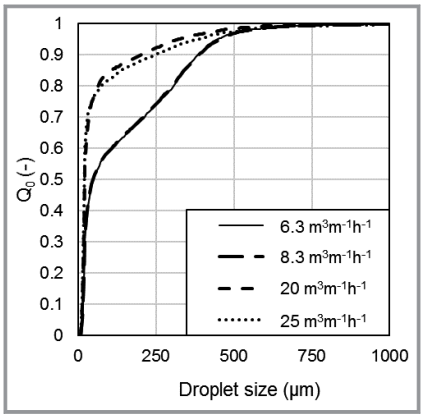


**Figure 6.** Liquid load effect on DSD (sieve tray; 1.5 $Pa^{0.5}$).

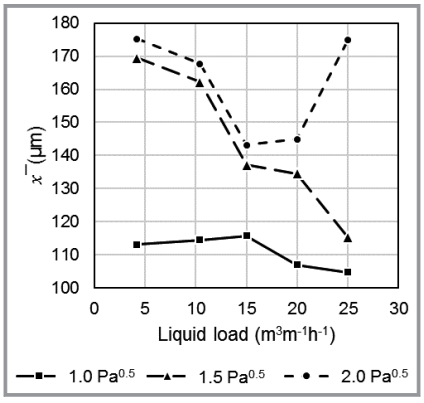


**Figure 7.** Average droplet diameter up to 25 $m^3m^{-1}h^{-1}$ liquid load (fixed valve tray; 1.5 $Pa^{0.5}$).

entrainment rates, which is in line with the findings of Kister and Haas [6] as well as Lockett et al. [11]. It is worth mentioning that this behavior can change depending on the tray type. For example, Puppich and Goedecke [2] acquire the same results for sieve, valve, tunnel-cap and crossflow trays but not for bubble cap trays, where entrainment rates first increase and then decrease at high liquid loads of 20–30 $m^3m^{-1}h^{-1}$ at 1.6 $Pa^{0.5}$. A comparison of both tray types is depicted in Fig. 8 at a constant gas factor of 1.5 $Pa^{0.5}$ and liquid loads up to 25 $m^3m^{-1}h^{-1}$ with respect to a measurement height of 342.5 mm above each tray.

In this case, the sieve tray generates smaller droplets than the fixed valve tray. Considering the results of Fig. 3, higher droplet sizes above the sieve tray are expected due to the higher amount of entrainment above the sieve tray quantified by the capture tray measurements. An alternative explanation for this unexpected behavior might be the tray geometry. The open area of a sieve tray hole is far smaller ($A_{h,sieve} = 9.5 \cdot 10^{-5}\,m^2$) compared to a fixed valve opening ($A_{h,valve} = 6.4 \cdot 10^{-4}\,m^2$). In conclusion, the fractional hole area of the sieve tray ($A_f = A_{h,total}/A_b$) amounts to $A_f = 5.7\,\%$, while the fixed valve tray comes up to $A_f = 6.7\,\%$. Investigations of Pinczewski and Fell [10] show that entrainment rates increase with a decrease of the fractional hole area, which is in line with the findings in Fig. 3, where the sieve tray tends to entrain more liquid to the capture tray than the fixed valve tray. In addition, the findings [29] show a decrease of droplet sizes above sieve trays with decreasing fractional hole areas $A_f$, which is in line with the findings from Fig. 8. A physical explanation for this behavior could be an increased breakdown of droplets above the sieve hole due to a higher velocity of the gas flow. A higher number of smaller droplets is being erupted out of the liquid phase possessing a higher kinetic energy and, thus, reaching the capture tray more often resulting in higher entrainment rates.

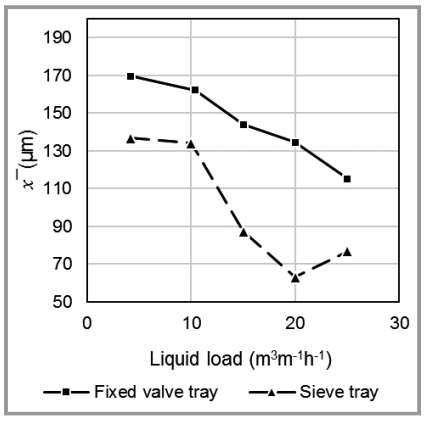


**Figure 8.** Average droplet diameter for both trays up to 25 $m^3m^{-1}h^{-1}$ liquid load (1.5 $Pa^{0.5}$).

An analysis of the number of detected droplets for each tray supports this hypothesis. For example, measurements at 20 $m^3m^{-1}h^{-1}$ liquid load and gas factor of 1.5 $Pa^{0.5}$ above the sieve tray detect 47.4 % more droplets compared to the fixed valve tray. The effect stays consistent among the remaining samples. A disadvantage of local measurement techniques like the modified OMOP is the local relevance of each measurement. Consequently, an integral coverage of the whole tray area would require measurements at a high number of positions. Fig. 9 depicts measurements at different radial positions above the sieve and fixed valve tray. This sample refers to a liquid load of 20 $m^3m^{-1}h^{-1}$ and a gas load of 1.2 $Pa^{0.5}$ (sieve tray) and 1.5 $Pa^{0.5}$ (fixed valve tray) at a measurement height of 342.5 mm. Concerning the radial positioning of the modified OMOP, the scaling of the horizontal axis is expressed as the measurement position within the column $r$ away from the center dependent on the diameter $R$ of the column. Consequently, the value zero on the horizontal axis stands for measurements at the tray center.

Measuring points across the column diameter with respect to the sieve tray show minor differences. The highest deviation between two positions amounts to $f_x = 20\,\%$ for the measuring positions 0 and (–)0.37 $r/R$. In contrast, measuring points across the column diameter with respect to the fixed valve tray show more obvious differences.

 © 2019 The Authors. Published by WILEY-VCH Verlag GmbH & Co. KGaA, Weinheim 

15222640, 2020, 3, Downloaded from https://onlinelibrary.wiley.com/doi/10.1002/cite.201900112 by Rheinland-Pfälzische Technische Universität Kaiserslautern-Landau, Wiley Online Library on [05/04/2024]. See the Terms and Conditions (https://onlinelibrary.wiley.com/terms-and-conditions) on Wiley Online Library for rules of use; OA articles are governed by the applicable Creative Commons License

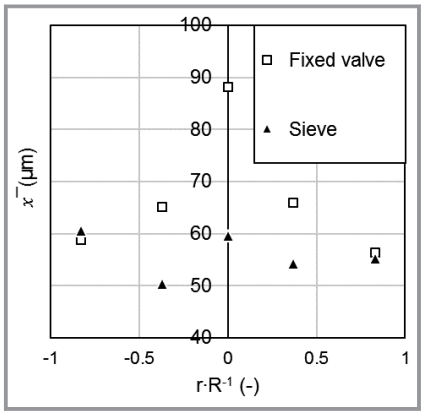


**Figure 9.** Average droplet diameter across tray area at 20 $m^3m^{-1}h^{-1}$ liquid load above sieve (1.5 $Pa^{0.5}$) and fixed valve tray (1.2 $Pa^{0.5}$).

Droplets in the column center are larger compared to areas closer to the column wall. Consequently, the highest deviation between two points amounts to $f_x$ = 56.1 % for the measuring points 0 and (+)0.83 $r/R$. Despite the lower gas load on the fixed valve tray, droplets above the sieve tray are in average still smaller leading to a maximum deviation at the center points (0 $r/R$) of $f_x$ = 47.8 %. It appears reasonable to conclude that the influence of the tray design also affects the droplet regime with respect to measurement positions away from the center especially near the column wall. DSD above the fixed valve tray show a clear wall tendency probably due to a lower gas velocity near the column wall. It is expected that the deflection of the gas flow caused by the valve construction has a distinct effect on the droplet regime compared to the sieve tray with its uniformly aligned sieve holes. The detection of smaller droplets above the fixed valve tray at ±0.83 $r/R$ emphasizes this hypothesis. Experiments depicted in Fig. 9 run at standard operation conditions in the froth regime. Measurements at low liquid loads (spray regime) or high gas loads (> 2 $Pa^{0.5}$) could reveal even stronger effects.

Experimental results depicted in Figs. 3a–9 demonstrate the wide application range of the modified OMOP for characterization of a dispersed liquid phase in absorption and distillation systems. With respect to entrainment, the probe holds the potential to quantify the amount of entrainment between two stages with a few measurements. Therefore, the entrainment extrapolation from Eqs. (5) and (6) calculates the amount of entrained liquid with aid of the detected droplet volume. A comparison with the quantified amount of entrained liquid from the capture tray is depicted in Fig. 10. The samples of Fig. 10a refer to measurements above the sieve tray at a constant liquid load of 6.3 $m^3m^{-1}h^{-1}$ and gas factors between 1 and 2.33 $Pa^{0.5}$. Runs with the modified OMOP are based on 7500 images at 40 Hz. A logarithmic plot of the vertical axis visualizes the differences between the single entrainment rates more clearly. The comparison between the conservative capture tray method and the entrainment estimation of the modified OMOP shows a satisfactory agreement. Concerning the four depicted gas factors in Fig. 10a, the relative deviation between both methods amounts to $f_{E_{eff}}$ = 15.6 %. The highest relative deviation goes back to the sample at 2.0 $Pa^{0.5}$ and comes up to $f_{E_{eff}}$ = 22.1 %. Fig. 10b refers to measurements above the fixed valve tray at a constant gas factor of 1.5 $Pa^{0.5}$ and liquid loads between 6.3 and 25 $m^3m^{-1}h^{-1}$.

The agreement between both measurement methods is again satisfactory. Relative deviation across the five depicted liquid loads amounts to $f_{E_{eff}}$ = 13.3 %. The sample at 20 $m^3m^{-1}h^{-1}$ shows the highest relative deviation of $f_{E_{eff}}$ = 23 %. The remaining deviation between the capture tray method and modified OMOP appears reasonable, as the capture tray is not able to entrain all droplets, while the modified OMOP is not able to exclude all falling droplets from the sample.

## 6 Conclusion

The presented modified OMOP is capable of analyzing dispersed liquids with a high precision demonstrated by investigation of monodisperse particles down to 9.18 µm and fast moving droplets down to 74.5 µm and up to 18.97 m $s^{-1}$. The DSD above sieve and fixed valve trays show a larger number of bigger droplets at increased gas factors. This effect stays constant over the whole design area of both trays and corresponds to entrainment quantification with the capture tray method. The effect of liquid load on entrainment is more complex but capture tray results clearly show

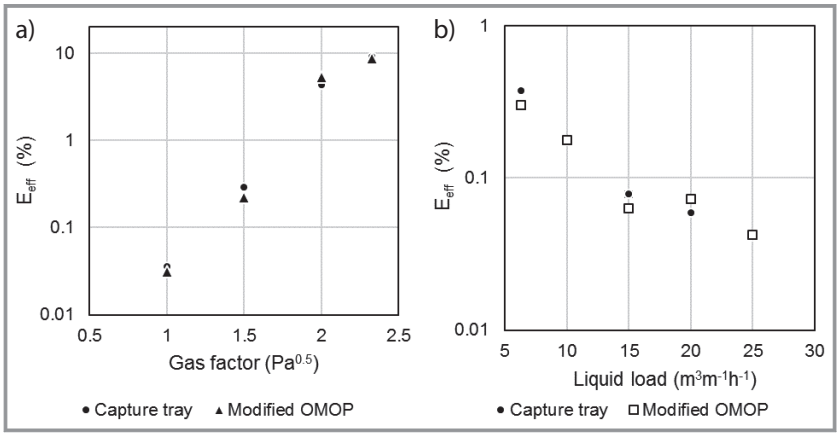


**Figure 10.** a) Entrainment quantification by modified OMOP compared to capture tray at different gas factors above sieve trays at a constant liquid load of 6.3 $m^3m^{-1}h^{-1}$. b) Entrainment quantification by modified OMOP compared to capture tray at different liquid loads above fixed valve tray at a constant gas factor of 1.5 $Pa^{0.5}$.

 © 2019 The Authors. Published by WILEY-VCH Verlag GmbH & Co. KGaA, Weinheim 

15222640, 2020, 3, Downloaded from https://onlinelibrary.wiley.com/doi/10.1002/cite.201900112 by Rheinland-Pfälzische Technische Universität Kaiserslautern-Landau, Wiley Online Library on [05/04/2024]. See the Terms and Conditions (https://onlinelibrary.wiley.com/terms-and-conditions) on Wiley Online Library for rules of use; OA articles are governed by the applicable Creative Commons License

a decreased amount of entrainment with increasing liquid loads followed by an increase of entrainment at very high liquid loads (20–25 $m^3m^{-1}h^{-1}$). The DSD reveal the same effect for both trays. Comparison of the DSD between sieve and fixed valve tray identify a lower average droplet diameter for the sieve tray compared to the fixed valve tray, although quantification with the capture tray shows higher entrainment rates for the sieve tray. A plausible explanation would be an enhanced number of smaller droplets generated by the smaller openings of the sieve tray. Image acquisition supports this assumption, as measurements above the sieve tray capture a larger number of droplets compared to the fixed valve tray. DSD across the column diameter at a constant liquid load of 20 $m^3m^{-1}h^{-1}$ and gas factors of 1.2 $Pa^{0.5}$ (sieve tray) and 1.6 $Pa^{0.5}$ (fixed valve tray) reveal smaller droplet diameters near the column wall in case of the fixed valve tray. Droplet sizes above the sieve tray remain rather constant most likely due to the uniformly alignment of the sieve holes. A comparison between entrainment rates acquired by capture tray and modified OMOP shows satisfactory agreements for measurements above both trays. Furthermore, the selection of the operation parameters with respect to Fig. 10 underlines the ability of the modified OMOP to estimate low (Fig. 10b) and high (Fig. 10a) entrainment rates on a reliable basis.

In summary, the modified OMOP is a powerful instrument for detection and analysis of dispersed liquid droplets in absorption and distillation columns due to its flexible application, fast performance, high precision and the wide application range in a large number of different systems. Especially the early development status of image-based optical measurement techniques emphasizes the high potential of these methods for the investigation and control of dispersed fluid flows. The probe enables an easy monitoring and control of entrainment using just one existing nozzle at the column shell. By investigation of the droplet regime, the modified OMOP helps to deepen the understanding of the fluid dynamics within the column due to the analysis of the fluid phase behavior. Therefore, successful measurements of DSD with image-based methods within the column represent the missing link between varying operation parameters and changes in entrainment rates. A deeper understanding of the mechanism operation parameter ↔ fluid dynamic behavior ↔ change in entrainment will be beneficial for future column design. The opportunity to quantify entrainment with a more cost efficient and flexible image-based method represents a serious potential for future process optimization especially in terms of energy costs and plant safety.

We wish to thank the German Federal Ministry for Economic Affairs and Energy for their financial support and our partners in the joint project TERESA.

## Symbols used

| | | |
|---|---|---|
| $A_b$ | [$m^2$] | bubbling tray area |
| $A_c$ | [$m^2$] | column cross sectional area |
| $A_f$ | [%] | fractional hole area = $A_{h,total}/A_b$ |
| $A_h$ | [$m^2$] | hole area |
| $A_{h,total}$ | [$m^2$] | total hole area |
| $A_{OMOP}$ | [$m^2$] | covered area by modified OMOP |
| $d$ | [µm] | droplet diameter |
| $d_h$ | [mm] | tray hole diameter |
| $\dot{E}'$ | [$m^3h^{-1}$] | extrapolated amount of entrainment |
| $E_{cap}$ | [%] | entrainment for tray capacity |
| $E_{eff}$ | [%] | entrainment for tray efficiency |
| $f_{cam}$ | [Hz] | camera acquisition frame rate |
| $f_{E_{eff}}$ | [%] | deviation of entrainment rates from capture tray and modified OMOP |
| $f_x$ | [%] | deviation of arithmetic means |
| $F$ | [$Pa^{0.5}$] | gas factor |
| $F_{crit}$ | [$Pa^{0.5}$] | critical flow factor |
| $g$ | [$m\,s^{-2}$] | gravitational force |
| $h_{valve}$ | [mm] | height of valve |
| $H_{cap}$ | [m] | distance OMOP to capture tray |
| $k$ | [–] | resistance coefficient |
| $\dot{L}$ | [$m^3h^{-1}$] | liquid flow across tray |
| $\dot{L}'$ | [$m^3h^{-1}$] | flow of entrained liquid |
| $h_w$ | [m] | outlet weir height |
| $l_w$ | [m] | outlet weir length |
| $Q_0$ | [–] | number cumulative distribution |
| $Q_3$ | [–] | volume cumulative distribution |
| $s$ | [variable] | standard deviation |
| $\dot{V}$ | [$m^3h^{-1}$] | flow of vapor |
| $V_d$ | [$m^3$] | detected droplet volume |
| $V_{meas}$ | [$m^3$] | measurement volume |
| $\bar{x}$ | [µm] | arithmetic mean of particle |
| $x_{50}$ | [µm] | median particle diameter |

## Greek symbols

| | | |
|---|---|---|
| $\rho_g$ | [$kg\,m^{-3}$] | gas density |
| $\rho_l$ | [$kg\,m^{-3}$] | liquid density |
| $\nu$ | [$m\,s^{-1}$] | velocity of continuous medium |

## Abbreviation

| | |
|---|---|
| DSD | droplet size distribution(s) |
| LED | light-emitting diode |
| OMOP | optical multimode online probe |
| PDA | phase Doppler anemometry |

## References

[1] E. C. Uys, C. E. Schwarz, A. J. Burger, J. H. Knoetze, *Chem. Eng. Res. Des.* **2012**, *90 (12)*, 2072–2085. DOI: https://doi.org/10.1016/j.cherd.2012.05.008

 © 2019 The Authors. Published by WILEY-VCH Verlag GmbH & Co. KGaA, Weinheim 

15222640, 2020, 3, Downloaded from https://onlinelibrary.wiley.com/doi/10.1002/cite.201900112 by Rheinland-Pfälzische Technische Universität Kaiserslautern-Landau, Wiley Online Library on [05/04/2024]. See the Terms and Conditions (https://onlinelibrary.wiley.com/terms-and-conditions) on Wiley Online Library for rules of use; OA articles are governed by the applicable Creative Commons License

[2] P. Puppich, R. Goedecke, *Chem. Eng. Technol.* **1987**, *10 (1)*, 224–230. DOI: https://doi.org/10.1002/ceat.270100127
[3] I. Paradissiadis, F. Widmer, *Chem. Eng. Process.* **1984**, *18 (5)*, 249–253. DOI: https://doi.org/10.1016/0255-2701(84)80008-2
[4] D. Staak, Absicherung von Destillationskolonnen im nicht bestimmungsgemäßen Bereich, *Dissertation*, Technische Universität Berlin **2010**.
[5] J. Stichlmair, H. Hofer, *Chem. Ing. Tech.* **1978**, *50 (7)*, 553. DOI: https://doi.org/10.1002/cite.330500717
[6] H. Z. Kister, J. R. Haas, *Ind. Eng. Chem. Res.* **1988**, *27 (12)*, 2331–2341. DOI: https://doi.org/10.1021/ie00084a018
[7] S. I. Cheng, A. J. Teller, *AIChE J.* **1961**, *7 (2)*, 282–287. DOI: https://doi.org/10.1002/aic.690070223
[8] A. P. Colburn, *Ind. Eng. Chem.* **1936**, *28 (5)*, 526–530. DOI: https://doi.org/10.1021/ie50317a005
[9] H. Z. Kister, J. R. Haas, *Inst. Chem. Eng. Symp. Ser.* **1988**, *104*, A483-A494.
[10] W. V. Pinczewski, N. D. Benke, C. J. D. Fell, *AIChE J.* **1975**, *21 (6)*, 1210–1213. DOI: https://doi.org/10.1002/aic.690210625
[11] M. J. Lockett, G. T. Spiller, K. E. Porter, *Trans. Inst. Chem. Eng.* **1976**, *54*, 202–204.
[12] J. Schulz, H.-J. Bart, *Chem. Eng. Res. Des.* **2019**, *147*, 624–633. DOI: https://doi.org/10.1016/j.cherd.2019.05.041
[13] M. Lichti, J. Schulz, H.-J. Bart, *Chem. Ing. Tech.* **2019**, *91 (4)*, 429–434. DOI: https://doi.org/10.1002/cite.201800045
[14] J. Schulz, H.-J. Bart, *Chem. Eng. Trans.* **2018**, *69*, 751–756. DOI: https://doi.org/10.3303/CET1869126
[15] M. Souders, G. G. Brown, *Ind. Eng. Chem.* **1934**, *26*, 98–103. DOI: https://doi.org/10.1021/ie50289a025
[16] R. de Villamil, *Resistance of Air*, E.&F.N. SPON LTD., 57 HAYMARKET, S.W., London **1917**.
[17] H. Z. Kister, W. V. Pinczewski, C. J. D. Fell, *Ind. Eng. Chem. Process Des. Dev.* **1981**, *20 (3)*, 528–532. DOI: https://doi.org/10.1021/i200014a024
[18] J. Fair, *Pet. Chem. Eng.* **1961**, *33 (10)*, 211–218.
[19] J. Stichlmair, A. Mersmann, *Chem. Ing. Tech.* **1977**, *49 (2)*, 106–117. DOI: https://doi.org/10.1002/cite.330490204
[20] C. Hunt, D. N. Hanson, C. R. Wilke, *AIChE J.* **1955**, *1 (4)*, 441–451. DOI: https://doi.org/10.1002/aic.690010410
[21] M. A. Jeronimo, H. Sawistowski, *Trans. Inst. Chem. Eng.* **1974**, *52*, 291–293.
[22] T. S. Banerjee, N. K. Roy, M. N. Rao, *Indian J. Technol.* **1969**, *7 (10)*, 308–311.
[23] D. L. Bennett, A. S. Kao, L. W. Wong, *AIChE J.* **1995**, *41 (9)*, 2067–2082. DOI: https://doi.org/10.1002/aic.690410907
[24] A. Koziol, J. Mackowiak, *Chem. Eng. Process.* **1990**, *27 (3)*, 145–153. DOI: https://doi.org/10.1016/0255-2701(90)87003-2.
[25] M. J. Lockett, *Distillation Tray Fundamentals*, Cambridge Univ. Press, Cambridge **1986**.
[26] A. J. Teller, R. E. Rood, *AIChE J.* **1962**, *8 (3)*, 369–372. DOI: https://doi.org/10.1002/aic.690080322
[27] M. Lichti, H.-J. Bart, *Chem. Ing. Tech.* **2017**, *89 (12)*, 1599–1610. DOI: https://doi.org/10.1002/cite.201700035
[28] K. Bauckhage, *Chem. Ing. Tech.* **1996**, *68 (3)*, 253–266. DOI: https://doi.org/10.1002/cite.330680306
[29] W. V. Pinczewski, C. J. D. Fell, *Trans. Inst. Chem. Eng.* **1977**, *55*, 46–52.
[30] M. Lichti, H.-J. Bart, *ChemBioEng Rev.* **2018**, *5 (2)*, 79–89. DOI: https://doi.org/10.1002/cben.201800001
[31] H.-J. Bart, M. W. Hlawitschka, M. Mickler, M. Jaradat, S. Didas, F. Chen, H. Hagen, *Chem. Ing. Tech.* **2011**, *83 (7)*, 965–978. DOI: https://doi.org/10.1002/cite.201100014
[32] M. Lichti, C. Roth, H.-J. Bart, *EP 3067685A1*, **2016**.
[33] A. Köhler, *Z. Wiss. Mikrosk. Mikrosk. Tech.* **1893**, *10 (4)*, 433–440.
[34] M. Mickler, H.-J. Bart, *Chem. Ing. Tech.* **2013**, *85 (6)*, 901–906. DOI: https://doi.org/10.1002/cite.201200139

 © 2019 The Authors. Published by WILEY-VCH Verlag GmbH & Co. KGaA, Weinheim 

15222640, 2020, 3, Downloaded from https://onlinelibrary.wiley.com/doi/10.1002/cite.201900112 by Rheinland-Pfälzische Technische Universität Kaiserslautern-Landau, Wiley Online Library on [05/04/2024]. See the Terms and Conditions (https://onlinelibrary.wiley.com/terms-and-conditions) on Wiley Online Library for rules of use; OA articles are governed by the applicable Creative Commons License